ANL-21/38

# Fabrication and Preliminary Demonstration of Microwave Resonant Cavity Transducer Performance

*Development of Sensor Performance Model of Microwave Cavity Flow Meter for Advanced Reactor High Temperature Fluids*

**Nuclear Science and Engineering Division**

ANL-21/38

# Fabrication and Preliminary Demonstration of Microwave Resonant Cavity Transducer Performance

*Development of Sensor Performance Model of Microwave Cavity Flow Meter for Advanced Reactor High Temperature Fluids*

prepared by
Alexander Heifetz[1], Sasan Bakhtiari[1], Eugene R. Koehl[1], David Aronson[1,2]

Nuclear Science Engineering Division, Argonne National Laboratory
University of Illinois at Urbana Champaign

August 31, 2021

# Table of Contents

Table of Contents ..... 1
List of Figures ..... 2
Abstract ..... 3
1. Introduction ..... 4
2. Fabrication of Sensor Prototype ..... 6
2.1. Fabrication of microwave cavity ..... 6
2.2. Fabrication of piping Tee adapter ..... 8
3. Preliminary Proof-of-Principle Tests ..... 11
3.1. Electronic measurement system assembly ..... 11
3.2. Proof-of-principle measurements ..... 12
4. Analysis of Sensor Mechanical Resilience ..... 14
4.1. Analytical model ..... 14
4.2. COMSOL numerical model ..... 16
5. Conclusions ..... 18
References ..... 19

# List of Figures

**Figure 1 –** (a) Conceptual drawing of waveguide-coupled microwave cylindrical cavity with flexible membrane. (b) Deflection of membrane due to dynamic fluid pressure changes cavity volume, which shifts microwave resonant frequency. ..... 4
**Figure 2 –** Side view and 3D visualization of the cylindrical cavity design ..... 6
**Figure 3 –** Top view of the cavity and 3D visualization of waveguide coupling cavity side wall 7
**Figure 4 –** Brass K-band cylindrical cavity fabricated for proof-of-principle studies ..... 7
**Figure 5 –** Brass cavity coupled to WR-42 bulkhead waveguide ..... 8
**Figure 6 –** Leak-proof assembly consisting of a piping Tee and WR-42 bulkhead waveguide for insertion of microwave cavity into fluid stream ..... 9
**Figure 7 –** Schematic drawing of adaptor for mounting WR-42 bullhead waveguide in a piping Tee ..... 9
**Figure 8 –** Photograph of adaptor and WR-42 bulkhead waveguide installed in piping Tee ..... 10
**Figure 9 –** Electronics and mechanics of the experimental setup for proof-of-principle testing. 11
**Figure 10 –** Waveguide microwave circulator is used for excitation and readout of microwave cavity ..... 12
**Figure 11 –** Spectral shift of microwave cavity resonant frequency due mechanical pressure on membrane. (a) f = 25.828GHz (marker 1) (b) f = 25.84GHz (marker 2) after applying pressure 13
**Figure 12 –** Model of a thin circular plate ..... 14
**Figure 13 –** Plot of $\sigma_{max}$ as a function of *h* for (a) v = 1m/s, (b) v = 0.5m/s ..... 15
**Figure 14 –** COMSOL claculation of Von Mises stresses for (a) v = 1 m/s, *h* = 10mil, (b) v = 0.5 m/s, *h* = 10mil, (c) v = 0.5 m/s, *h* = 5mil. ..... 17

## Abstract

We are investigating a microwave cavity-based transducer for in-core high-temperature fluid flow sensing in molten salt cooled reactors (MSCR) and sodium fast reactors (SFR). This sensor is a hollow metallic cylindrical cavity, which can be fabricated from stainless steel, and as such is expected to be resilient to radiation, high temperature and corrosive environment of MSCR and SFR. The principle of sensing consists of making one wall of the cylindrical cavity flexible enough so that dynamic pressure, which is proportional to fluid velocity, will cause membrane deflection. Membrane deflection causes cavity volume change, which leads to a shift in the resonant frequency. We have developed an initial design for proof-of-principle testing of the flow sensor performance in microwave K-band. A cylindrical resonator prototype was fabricated from brass for initial tests in water. The cavity size is matched to the flange of a standard WR-42 waveguide. Microwave field is coupled into the resonant cavity through a subwavelength-size aperture. A test article was developed, consisting of a piping Tee with bulkhead WR-42 microwave waveguide installed in leak-proof design. In the test article, the cylindrical cavity is positioned in the center of the pipe. A microwave waveguide circulator was installed in the setup to suppress microwave reflections at the cavity entrance. Preliminary spectral characterization of cavity spectral response was performed with microwave VNA. Applying mechanical pressure to cavity membrane showed a measurable shift in the microwave resonant frequency. We also investigate mechanical integrity of the flowmeter's membrane through computer simulations. By calculating the stress on the plate due to deflection and, comparing the stress to the material ultimate tensile strength and yield strength, it can be estimated if the plate will fail. The stress on the plate was calculated with an analytic closed form solution model, and with COMSOL Structural Mechanics Module which does not involve any approximations. Both the analytic model and COMSOL model showed that maximum stresses on the plate, which are at the radial boundary of the plate, are three orders of magnitude smaller than the yield strength and ultimate tensile strength. This indicates that the sensor is at a low risk of mechanical failure.

# 1. Introduction

High-temperature fluid reactors, such as sodium fast reactors (SFR) and molten salt cooled reactors (MSCR) are a promising advanced reactor option with highly efficient thermal energy conversion cycle [1,2]. Measurement of high-temperature fluid process variables, in particular the flow inside the pressure vessel, is a challenging task because of harsh environments of advanced reactors, which includes radiation, high temperature, and contact with highly corrosive coolant fluid. Molten salt flow sensors are typically ultrasonic ones [3]. Ultrasonic transducers are typically placed outside the vessel and pipes, but sensing requires a direct line-of-sight between the transducers. We are investigating a microwave cavity-based transducer for high-temperature fluid flow sensing for in-core sensing [4,5]. This sensor is a hollow metallic cavity, which can be fabricated from stainless steel, and as such is expected to be resilient to radiation, high temperature and corrosive environment of SFR and MSCR. A schematic drawing of the flow sensor is shown in Figure 1. The principle of sensing consists of making one wall of the cylindrical resonant cavity flexible enough so that dynamic pressure, which is proportional to fluid velocity, will cause membrane deflection. A cavity is characterized by its resonant frequencies, which occur due to constructive interferences of microwave field inside the cavity. Membrane deflection causes cavity volume change, and thus a shift in the resonant frequency. Using signal readout from microwave frequency shift in a hollow cavity is advantageous for applications in high temperature and high radiation environment, because no electronic components are placed inside the transducer. Energy coupling to and from the sensor will be achieved through a microwave waveguide, which will be an integral part of the insertion probe. A waveguide is a rigid narrow hollow metallic tube resilient to high temperature and high-radiation environment. In the drawing in Figure 1, microwave field is coupled into the cylindrical resonant cavity through a side wall.

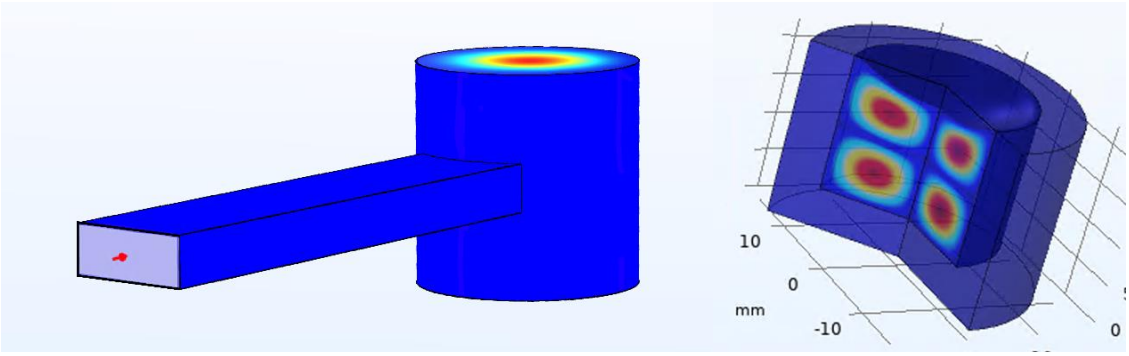


(a) (b)

**Figure 1 –** (a) Conceptual drawing of waveguide-coupled microwave cylindrical cavity with flexible membrane. (b) Deflection of membrane due to dynamic fluid pressure changes cavity volume, which shifts microwave resonant frequency.

The work described in this report consists of fabrication of K-band microwave cavity prototype for proof-of-principle flowmeter tests in water. Cylindrical cavity with the size matching the dimensions of a standard WR-42 waveguide flange was fabricated from brass for initial performance characterization. The cavity was coupled to a bulkhead WR-42 waveguide, which

was connected to a waveguide microwave circulator. The circulator was installed in the setup to suppress microwave reflections at the cavity entrance. A test articled with leak-proof insertion of microwave electronics into a piping Tee was developed. Preliminary spectral characterization of cavity spectral response was performed with microwave VNA. Applying mechanical pressure to cavity membrane showed a measurable shift in the microwave resonant frequency. When pressure is released, cavity spectrum returns to the original state, indicating that measurements are repeatable.

We also investigate mechanical integrity of the flowmeter's membrane through computer simulations. By calculating the stress on the plate due to deflection and, comparing the stress to the material ultimate tensile strength and yield strength, it can be estimated if the plate will fail. The stress on the plate was calculated with an analytic closed form solution model, and with COMSOL Structural Mechanics Module which does not involve any approximations. Both the analytic model and COMSOL model showed that maximum stresses on the plate, which are at the radial boundary of the plate, are three orders of magnitude smaller than the yield strength and ultimate tensile strength. This indicates that the sensor is at a low risk of mechanical failure.

# 2. Fabrication of Sensor Prototype

## 2.1. Fabrication of microwave cavity

Based on the results obtained from modeling and simulation of resonant transducer performance, preliminary design of the microwave cavity transducer was developed for fabrication in a machine shop [5]. The side view of the cavity is shown in Figure 2. All dimensions are in units of inches. In this design, the cavity is assembled with screws from a hollow cylinder, a thick cap at the bottom, and a thin diaphragm made from 10mil shim stock metal (1mil = $10^{-3}$in). The thin diaphragm is held in place with a clamping ring. All the holes in the drawing are for 4-40 screws, which are the same size screws used for K-band waveguide flange. In the design shown in Figure 2, microwave field is coupled into the cavity through a subwavelength aperture on the side of the cylinder. Compared to earlier design with 0.116in (3mm), a smaller diameter of the aperture 0.086in (2.2mm) was chosen. For K-band mean frequency $f_{mean}$ = 22GHz and corresponding free space wavelength $\lambda$ = 13.6mm, the diameter of the new aperture is 0.16$\lambda$. According to computer simulations, the Q factor of $TE_{012}$ mode would be higher for the smaller aperture. The aperture is matched to the center of the waveguide. Coupling of waveguide to the cylindrical cavity is accomplished by chamfering the side of a cylindrical cavity to obtain a flat surface. 3D rendering of the cylindrical cavity in Figure 2 shows the chamfered side surface and the small aperture for coupling microwave field into cavity.

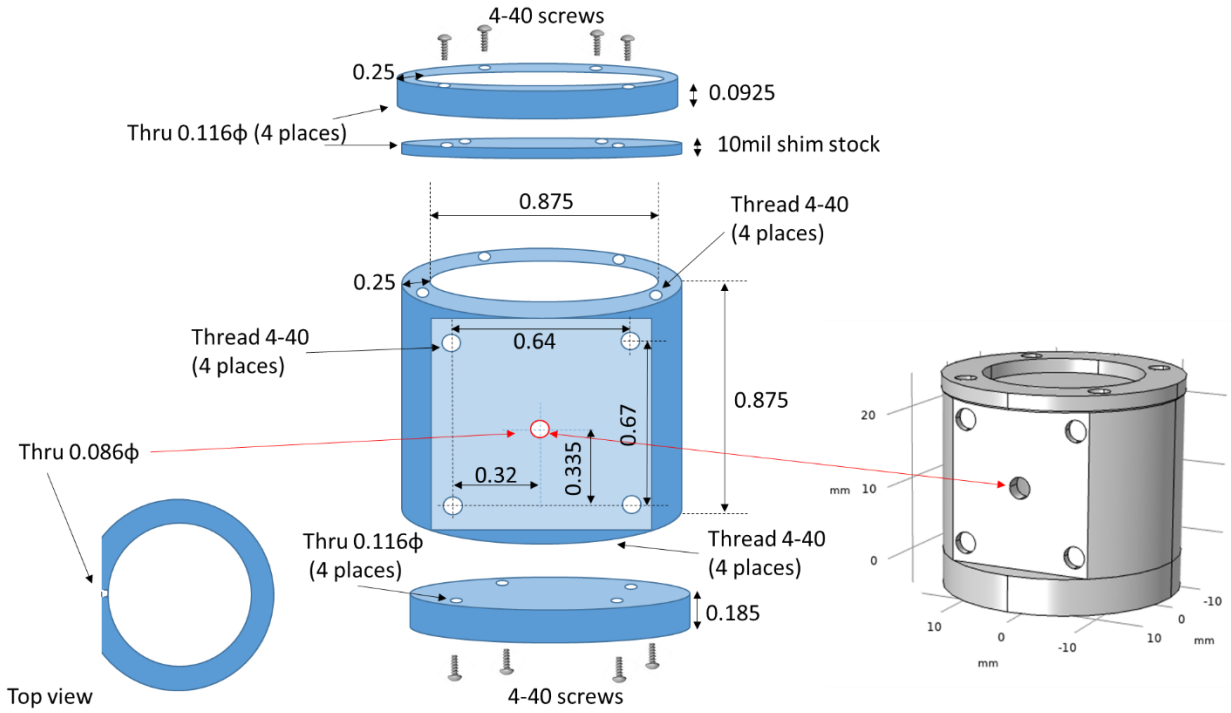


**Figure 2 –** Side view and 3D visualization of the cylindrical cavity design

Visualization of WR-42 microwave K-band waveguide attached to cylindrical cavity is shown in Figure 10. The top view of the cylinder without the diaphragm is also shown in Figure 3. In

addition to the diameter of the aperture, another parameter influencing efficiency of microwave coupling into cavity is the thickness of the aperture screen. Selecting aperture thickness involves a tradeoff between coupling efficiency and mechanic structural integrity of the resonator. Compared to initial cavity design with aperture thickness of 0.0925in (2.3mm), cavity dimensions were modified to design a structure with aperture thickness of 0.02in (0.5mm). Thickness of the new aperture is approximately 0.04λ. The drawing of the cavity with new dimensions is shown in Figure 3.

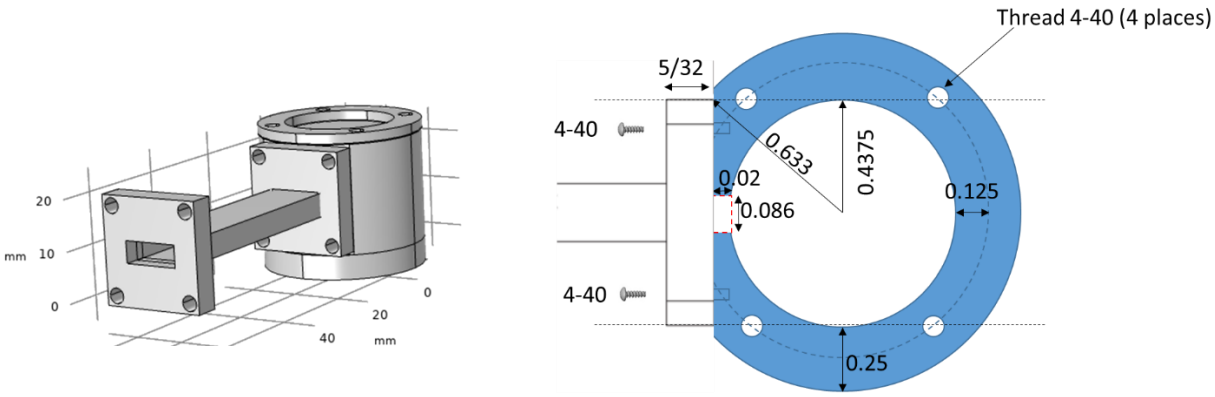


**Figure 3 –** Top view of the cavity and 3D visualization of waveguide coupling cavity side wall

For proof-of-principle study, a cavity was fabricated from brass. Using brass instead of stainless steel saves cost on materials and machining. K-band brass cavity fabricated at Argonne Central Shop is shown in Figure 4. The left panel shows a photograph of the cavity with the top membrane removed. The panel on the right shows an assembled cylindrical cavity with stainless steel screws. With this design, the top membrane is interchangeable. The cavity in Figure 4 has a 10mil-thick membrane. In addition 9mil and 8mil-thick membranes have been fabricated for flow sensor performance testing.

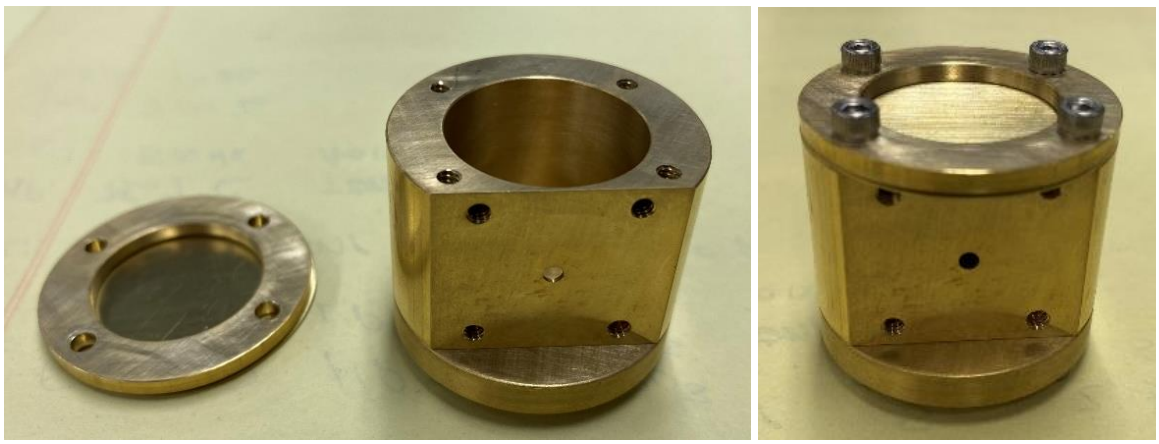

**Figure 4 –** Brass K-band cylindrical cavity fabricated for proof-of-principle studies

The photograph in Figure 5 shows the microwave cavity coupled to a commercial WR-2 bulkhead waveguide. The waveguide is welded to a mounting plate for leak-proof insertion of microwave flow sensor into a pipe.

**Figure 5 –** Brass cavity coupled to WR-42 bulkhead waveguide

## 2.2. Fabrication of piping Tee adapter

A leak-proof assembly for insertion of microwave cavity into a flow stream was designed using a bulkhead WR-42 transducer and a PVC size 3 piping reducing Tee. The adaptor is thick disc with a concentric hole. The schematics and dimensions of the assembly cross-section are shown in drawing in Figure 6. The location of the adaptor is indicated with solid grey color. The adaptor rests against the notches in the pipe of the Tee near the intersection. The dimensions were chosen to position the cylindrical resonant cavity in the middle of size 3 pipe. The outer diameter of the adaptor matches the dimensions of the mounting plate of the WR-42 bulkhead waveguide. The inner diameter is large enough for insertion of cylindrical cavity into the piping Tee. The adaptor was machined from solid PVC cylinder in Argonne Central Shop.

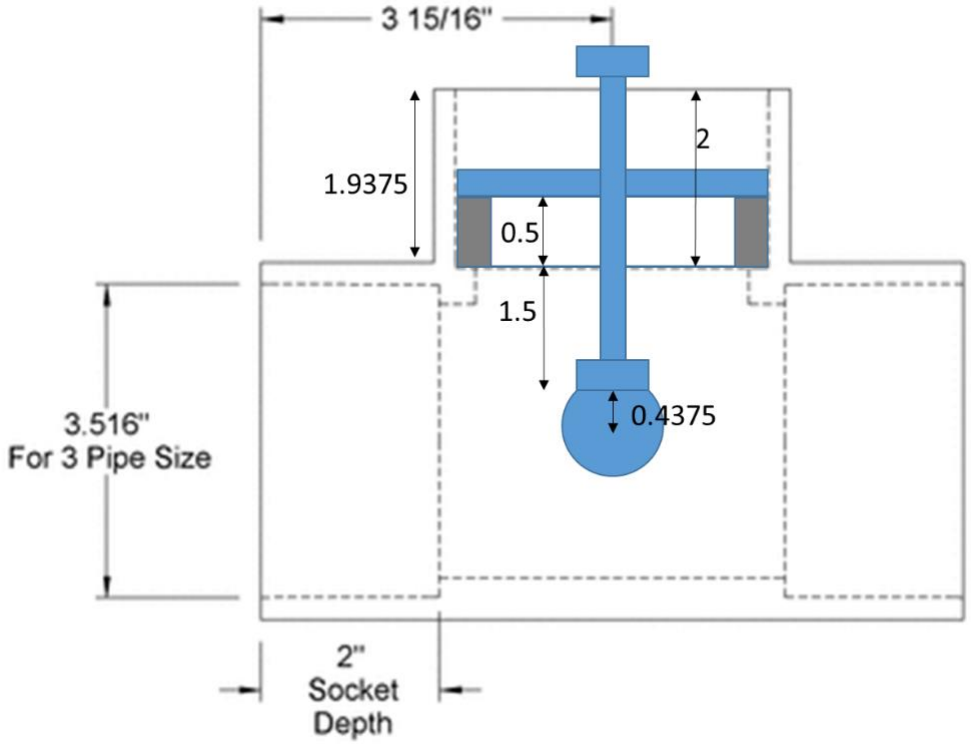


**Figure 6 –** Leak-proof assembly consisting of a piping Tee and WR-42 bulkhead waveguide for insertion of microwave cavity into fluid stream

Schematic drawing of the adaptor with all dimensions is shown in Figure 7. The adaptor is designed to fit inside size 3 pipe. The pattern of threaded blind holes in the adaptor is matched to that of the through holes on the mounting plate of the bulkhead waveguide.

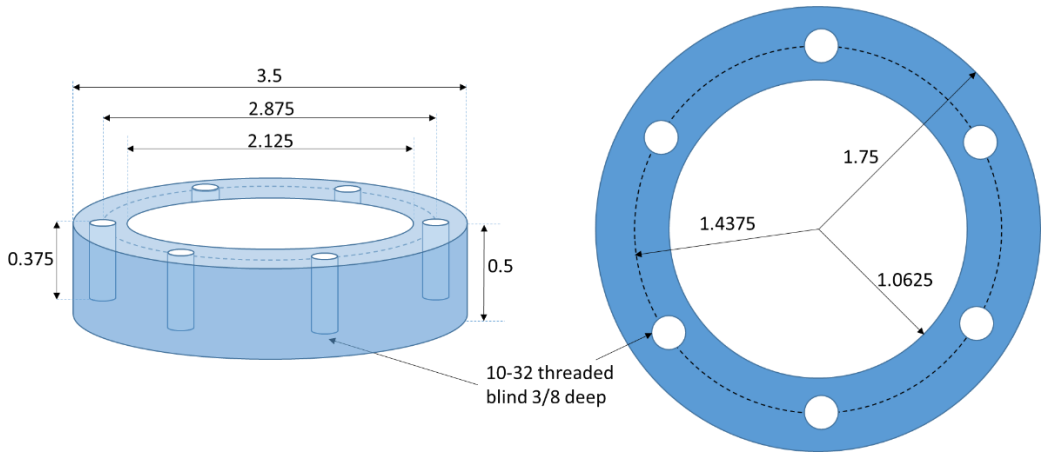


**Figure 7 –** Schematic drawing of adaptor for mounting WR-42 bullhead waveguide in a piping Tee

Photograph of the PVC adaptor and WR-42 bulkhead waveguide installed in clear PVC piping Tee is shown in Figure 8. The adaptor is glued into the piping Tee. The photograph is taken before the mounting plate was attached with screws to the adaptor plate.

**Figure 8 –** Photograph of adaptor and WR-42 bulkhead waveguide installed in piping Tee

# 3. Preliminary Proof-of-Principle Tests

## 3.1. Electronic measurement system assembly

Experimental setup consisting of the piping test article, microwave flow sensor, and microwave spectrum analyzer, is shown in Figure 9. In the setup, the cylindrical cavity is position in the middle of a PVC pipe with a bulkhead waveguide mounted on the side of the piping Tee. SMA (sub-miniature type A) cables are connecting the waveguide to VNA (vector network analyzer). Readout of the cavity spectrum is performed with a WR-42 waveguide microwave circulator, which isolates microwave reflection at the input to the cavity from microwave radiation of the cavity. Because microwave field is coupled into the cavity through a subwavelength hole, most of microwave power is reflected at the entrance to the cavity. If not suprressed, the reflected signal will overlap with radiation from the cavity, thus contributing a strong background to the signal measured with VNA.

**Figure 9 –** Electronics and mechanics of the experimental setup for proof-of-principle testing

Microwave circulator connected to the waveguide is shown in better details in zoomed-in image in Figure 10. SMA cable from VNA Port 1 is connected to the input (port 1) of the circulator.

Port 2 of the ciruclator is connected to the the waveguide. Port 3 of the circulator is to VNA port 2 with a cable marked with red tape. The signal measured with VNA is $S_{21}$. Isolation between circulator ports is approximately 20dB. Therefore, there is leakage of back-reflected signal which contributes to $S_{21}$ backgroud.

**Figure 10 –** Waveguide microwave circulator is used for excitation and readout of microwave cavity

## 3.2. Proof-of-principle measurements

Preliminary measurements of transducer signal was recorded with VNA as $S_{21}$ signal, which is shown in Figures 11(a) and 11(b). Frequency sweep is from 25.8GHz to 25.9GHz. In Figure 11(a), marker 1 indicates spectral location of the cavity $TE_{012}$ resonant frequency at f = 25.828GHz. Other spectral fluctuations observed in Figure 11(a) are most likely due to leakage through the circulator of the signal resulting from microwave reflection at cavity entrance. When a slight mechanical force applied with the dull end of a screw driver on the top thin membrane of the cylindrical cavity, $TE_{012}$ mode resonant frequency shifts to f = 25.84GHz. This spectral location is indicated with maker 2 in Figure 11(b). When the load is removed, frequency response returns to that of Figure 11(a).

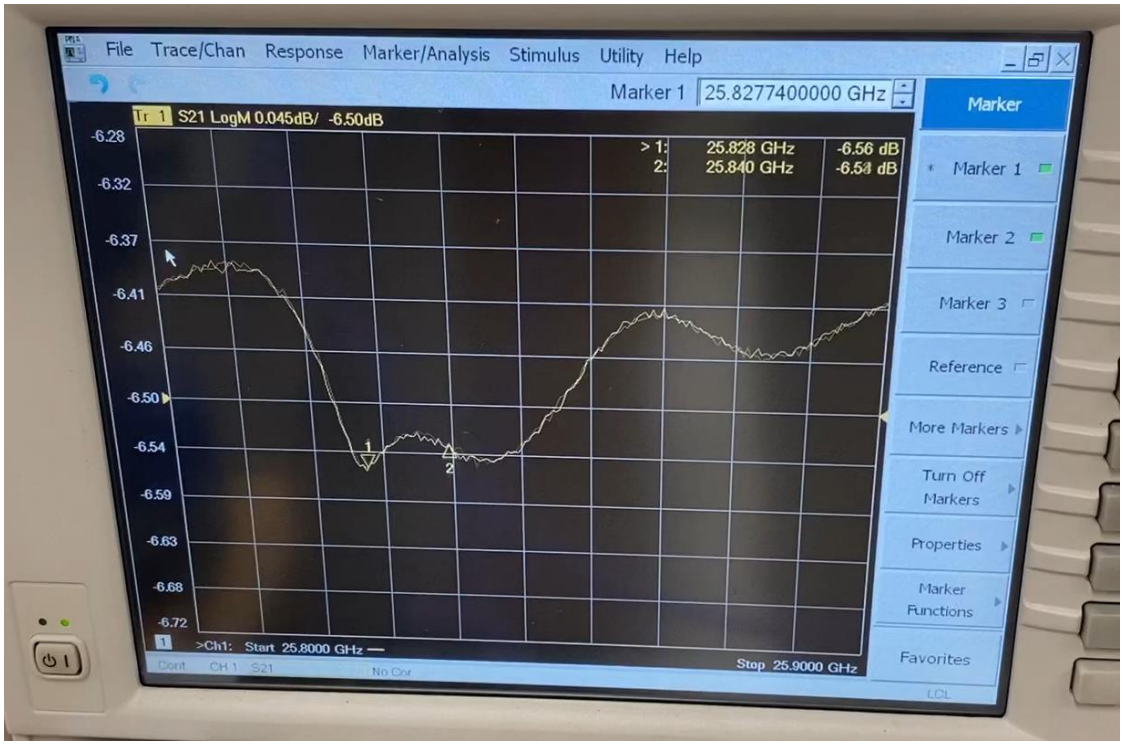


(a)


(b)

**Figure 11 –** Spectral shift of microwave cavity resonant frequency due mechanical pressure on membrane. (a) f = 25.828GHz (marker 1) (b) f = 25.84GHz (marker 2) after applying pressure

# 4. Analysis of Sensor Mechanical Resilience

## 4.1. Analytical model

In analyzing mechanical integrity of the membrane of the transducer shown in Figure 1, it is sufficient to consider an isolated model of a uniformly loaded thin stainless-steel circular plate fixed at the radial boundary. An example of a thin circular plate is show in Figure 12. The objective is to determine if for the sensor membrane dimensions and flow rates identified in prior work [4,5], maximum stresss on the membrane exceed YS and UTS values. For stainless steel 316, YS = 290 MPa and UTS = 580 MPa [4].

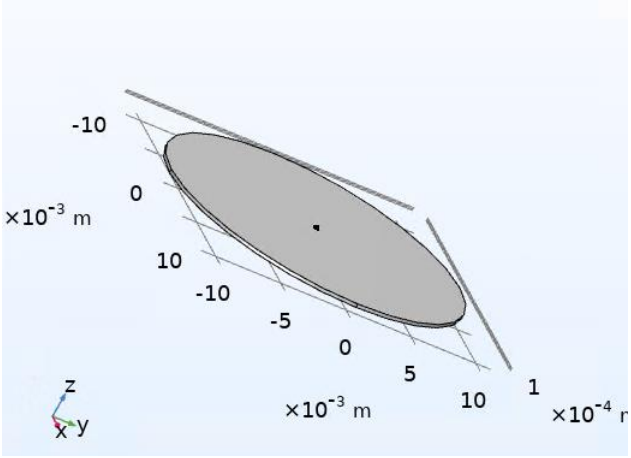


**Figure 12 –** Model of a thin circular plate

The plate in Figure 12 has radius *a* and thickness *h*. In the analysis of this report, radius is fixed with the value *a* = 11.1mm. Thickness *h* is in the range of 10mil to 5mil. A closed form analytic solution for deflection of the plate has been developed in literature [6]. The maximum stress on the plate is at the radial boundary, and is given as

$$\sigma_{\max} = \frac{3}{4} q \frac{a^2}{h^2} \tag{1}$$

Where *q* is the pressure on the plate. Dynamic fluid pressure is related to fluid velocity and density according to Bernoulli's equation

$$q = \frac{1}{2} \rho \mathbf{v}^2 \tag{2}$$

Where $\rho$ and v are the fluid densty and velocity, respectively. The maximum stress is weakly dependent on temperature through temperature-dependent fluid density. For example, for FLiBe ($LiF\text{-}BeF_2$), density correlation in units of $kg/m^3$ is given by [7]

$$\rho = 2415.6 - 0.49072T \tag{3}$$

Where *T* is in units of K. The correlation is valid for $732.2K<T<4498.8K$. Density changes by less than 1% for 100K temperature change. Water density at 20°C is $1000kg/m^3$, while density of liquid

sodium at 530ºC is 828kg/m$^3$ [8], and density of FLiBe at 550ºC is 2012kg/m$^3$ [9]. For order of magnitude calculations, differences in fluid densities by a factor of two can be neglected.

The graph in Figure 3 shows a plot of $\sigma_{max}$ as a function of *h* for representative velocity values [10] of v = 1 m/s in Figure 3(a) and v = 0.5m/s in Figure 13(b). The fluid is taken to be water at room temperature. The maximum stresses in Figures 13(a) and 13(b) are approximately 3MPa and 0.7MPa, respectively. These values are three orders of magnitude smaller than YS and UTS of stainless steel, which suggests that the risk of mechanical failure is low.

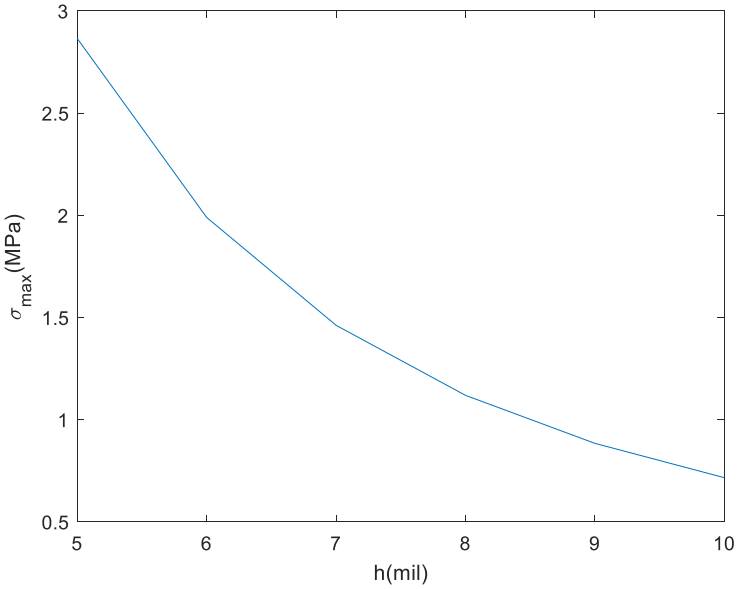


(a)

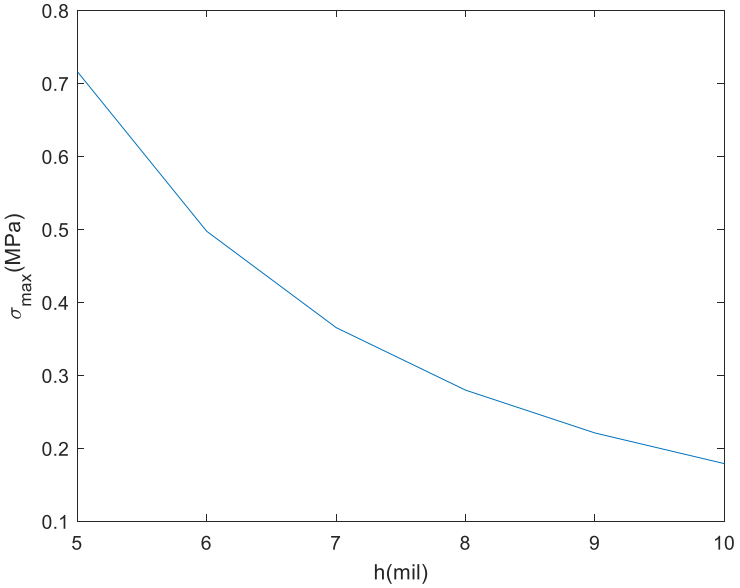


(b)

**Figure 13 –** Plot of $\sigma_{max}$ as a function of *h* for (a) v = 1m/s, (b) v = 0.5m/s

## 4.2. COMSOL numerical model

A numerical COMSOL model of a thin cicular radially constrained plate under uniform load was constructed to calculate the von Mises Stress, which is a value used to determine if a given material will yield or fracture. The plate was in room temperature conditions, and pressure calculations assume the fluid is water. In COMSOL calculations, resulting von Mieses stresses are displayed with as pseudo-color map of the circular plate. For the three simulation cases displayed in Figure 14, the radius of stainless steel 316 plate is a = 11.1mm. For the case in Figure 14(a), v = 1 m/s and *h* = 10mil, in Figure 14(b) v = 0.5 m/s, *h* = 10mil, and in Figure 4(c) v = 0.5 m/s, *h* = 5mil.

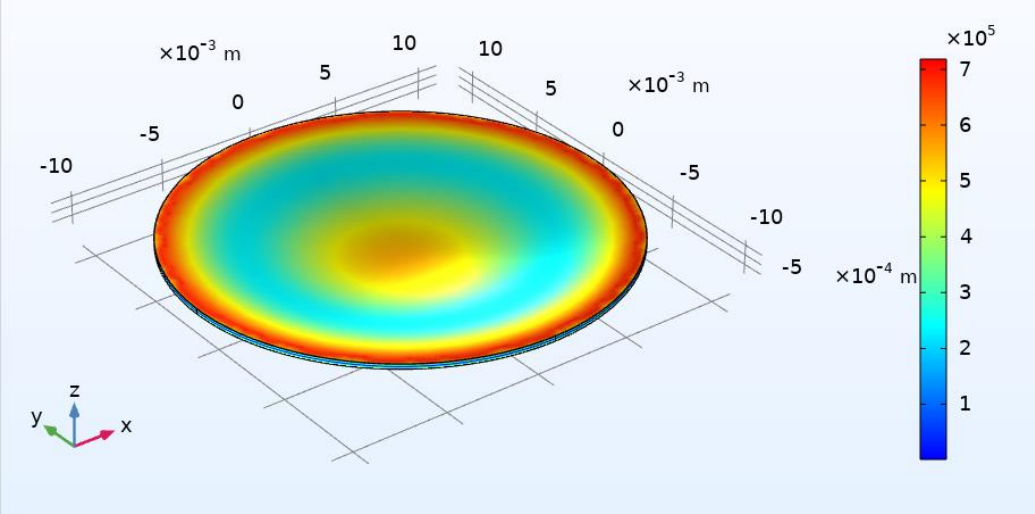


(a)

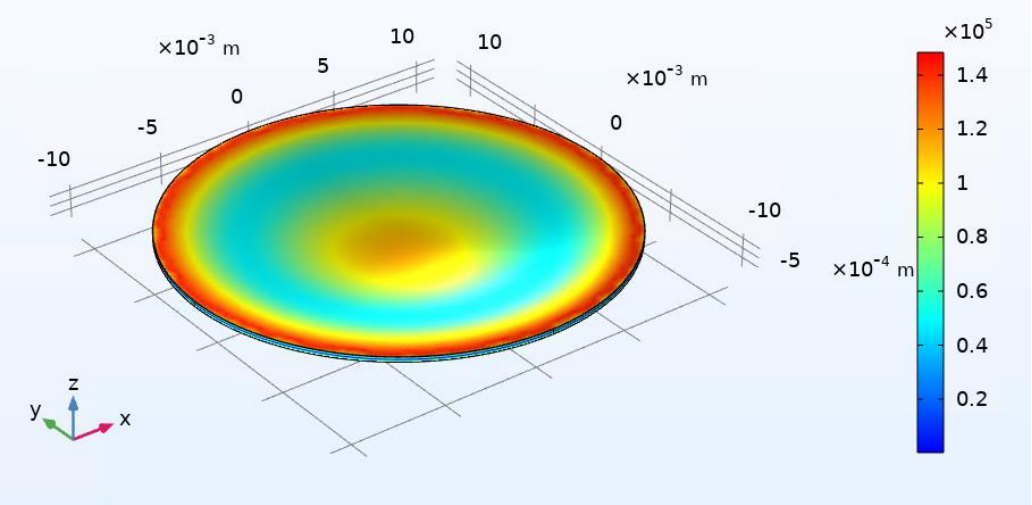


(b)

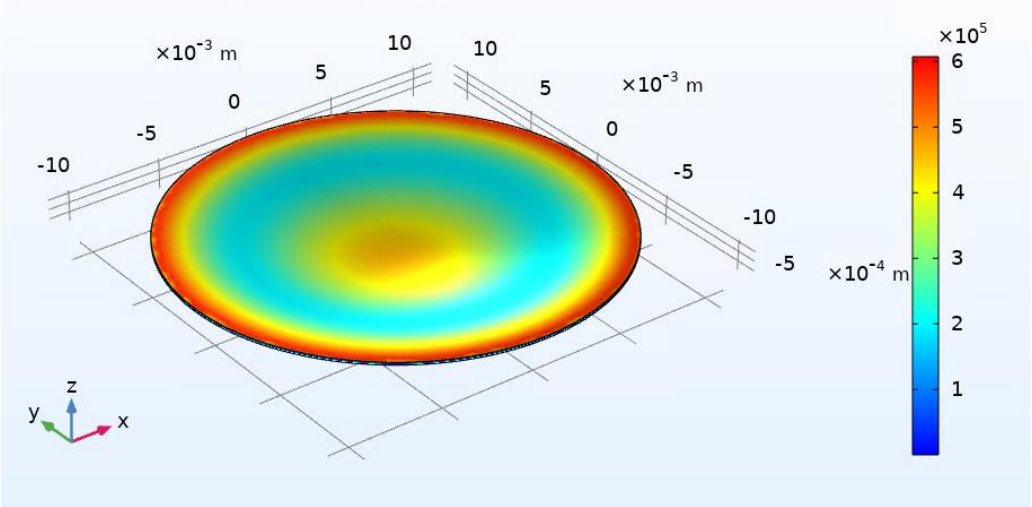


(c)

**Figure 14 –** COMSOL claculation of Von Mises stresses for (a) v = 1 m/s, *h* = 10mil, (b) v = 0.5 m/s, *h* = 10mil, (c) v = 0.5 m/s, *h* = 5mil.

The maximum von Mises Stress are approximately 0.7MPa, 0.14MPa, and 0.6MPa in Figures 14(a), 14(b), and 14(c). In comparison, $\sigma_{max}$ values calculated using Equation (1) for the same set of v and *h* values are 0.7MPa, 0.18MPa, 0.7MPa, respectively. The values obtained from COMSOL simulations and the analytic model are in good agreement. These values of maximum stress are three orders of magnitude smaller than the YS or UTS of stainless steel 316. This suggests that the membrane is at a low risk of fracture.

## 5. Conclusions

We describe development of a K-band microwave cylindrical cavity for preliminary proof-of-principle tests. Cylindrical cavity was fabricated from brass, and connected to WR-42 bulkhead waveguide. A microwave circulator was installed in the setup to suppress microwave reflections at the cavity entrance. A test articled with leak-proof insertion of microwave electronics into a piping Tee was developed. Preliminary spectral characterization of cavity spectral response was performed with microwave VNA. Applying mechanical pressure to cavity membrane showed a measurable shift in the microwave resonant frequency. When pressure is released, cavity spectrum returns to the original state, indicating that measurements are repeatable.

We also performed analytical and computational investigation of mechanical integrity of the sensor membrane. The mechanical model of the transducer membrane is a thin radially clamped circular plate subjected to uniform load. Stresses on the membrane are calculated with an analytic model, and with numerical COMSOL model. Maximum stresses on the plate are compared to yield strength (YS) and ultimate tensile strength (UTS) to determine if the plate could undergo plastic deformation or failure. Calculated maximum stresses are three orders of magnitude smaller than the YS and UTS. This indicates that the sensor should operate in the linear elastic deflection regime, and the likelihood of failure is relatively small.

Future work will involve measurements of spectral shift with calibrated load, will consist of either calibrated weights or water column. These measurements will produce a calibration curve, which will be compared with results obtained from computer simulations. Finally, the piping Tee will be inserted into a water flow loop, where the flow sensor will be used to measure fluid velocity. In parallel, signal processing algorithms will be developed to improve visibility of displayed signals.

## References


1. E. Blandford, K. Brumback, L. Fick, C. Gerardi, B. Haugh, E. Hillstrom, K. Johnson, P.F. Peterson, F. Rubio, F.S. Sarikurt, S. Sen, H. Zhao, N. Zweibaum, "Kairos Power Thermal Hydraulics Research and Development," Nuclear Engineering and Design 364, 110636 (2020).
2. K. Aoto, P. Dufour, Y. Hongyi, J. P. Glatz, Y. Kim, Y. Ashurko, R. Hill, N. Uto, "A Summary of Sodium-Cooled Fast Reactor Development," Progress in Nuclear Energy 77, 247-265 (2014).
3. D. Holcomb, R. Kisner, S. Cetiner, "Instrumentation Framework for Molten Salt Reactors," ORNL/TM-2018/868 (2018).
4. A. Heifetz, V. Ankel, D. Shribak, S. Bakhtiari, A. Cilliers, "Microwave Resonant Cavity-Based Flow Sensor for Advanced Reactor High Temperature Fluids," 12th Nuclear Plant Instrumentation, Control and Human-Machine Interface Technologies (NPIC-HMIT 2021) (2021).
5. A. Heifetz, D. Shribak, S. Bakhtiari, E.R. Koehl, "Design of Microwave Resonant Cavity Transducer," Argonne National Laboratory ANL-21/15 (2021).
6. S. Timoshenko and S. Woinowsky-Krieger, *Theory of Plates and Shells*, 2nd Edition, McGraw- Hill, New York, (1964).
7. G.L. Hoffman, M.C. Billone, J.F. Koening, J.M. Kramer, J.D.B. Lambert, L. Leibowitz, Y. Orechwa, D.R. Pedersen, D.L. Porter, H. Tsai, and A.E. Wright, "Metallic Fuels Handbook," ANL-NSE-3 (2019).
8. J.K. Fink and L. Leibowitz, "Thermodynamic and Transport Properties of Sodium Liquid and Vapor," ANL/RE-95/2 (1995).
9. M.S. Sohal, M.A. Ebner, P. Sabharwall, P. Sharpe, "Engineering Database of Liquid Salt Thermophysical and Thermochemical Properties," INL/EXT-10-18297 (2010).
10. D. Kultgen, C. Grandy, E. Kent, M. Weathered, D. Andujar, and A. Reavis, "Mechanisms Engineering Test Loop – Phase I Status Report – FY2018," ANL-ART-148, ANL-METL-14 (2018).

**Nuclear Science and Engineering (NSE) Division**
Argonne National Laboratory
9700 South Cass Avenue, Bldg. 208
Argonne, IL 60439

www.anl.gov